CHIN. PHYS. LETT. Vol. 38, No. 1 (2021) 017401

Superconducting Properties and Absence of Time Reversal Symmetry Breaking in the Noncentrosymmetric Superconducting Compounds $Ta_xRe_{1-x}(0.1 \leq x \leq 0.25)$

Chun-Qiang Xu(徐春强)[1], Yi Liu(刘艺)[2], Wei Zhou(周苇)[3], Jia-Jia Feng(冯嘉嘉)[1], Sen-Wei Liu(刘森巍)[1], Yu-Xing Zhou(周宇星)[4], Hao-Bo Wang(汪浩波)[3], Zhi-Da Han(韩志达)[3], Bin Qian(钱斌)[3], Xue-Fan Jiang(江学范)[3], Xiao-Feng Xu(许晓峰)[2,3], Wei Ye(叶巍)[1], Zhi-Xiang Shi(施智祥)[1*], Xiang-Lin Ke(柯祥林)[5*], and Pabitra-Kumar Biswas[6*]

[1] *School of Physics and Key Laboratory of MEMS of the Ministry of Education, Southeast University, Nanjing 211189, China*
[2] *Department of Applied Physics, Zhejiang University of Technology, Hangzhou 310023, China*
[3] *School of Electronic and Information Engineering, Changshu Institute of Technology, Changshu 215500, China*
[4] *Department of Physics, Zhejiang University, Hangzhou 310007, China*
[5] *Department of Physics and Astronomy, Michigan State University, East Lansing, Michigan 48824-2320, USA*
[6] *ISIS Pulsed Neutron and Muon Source, STFC Rutherford Appleton Laboratory, Harwell Campus, Didcot, Oxfordshire OX11 0QX, United Kingdom*

(Received 28 October 2020; accepted 13 November 2020; published online 6 January 2021)

Unconventional superconductivity, in particular, in noncentrosymmetric systems, has been a long-sought topic in condensed matter physics. Recently, Re-based superconductors have attracted great attention owing to the potential time-reversal symmetry breaking in their superconducting states. We report the superconducting properties of noncentrosymmetric compounds Ta_xRe_{1-x} with $0.1 \leq x \leq 0.25$, and find that the superconducting transition temperature reaches a maximum of $\sim$8 K at the optimal level $x = 0.15$. Nevertheless, muon-spin rotation and relaxation measurements reveal no time-reversal symmetry breaking existing in its superconducting state, which is in sharp contrast to both centrosymmetric Re metal and many other noncentrosymmetric Re-based superconductors.

DOI: 10.1088/0256-307X/38/1/017401

Understanding the effects of broken spatial inversion symmetry on the electron pairing in superconducting states with a noncentrosymmetric crystal structure has attracted considerable attention. The absence of inversion symmetry can lead to an antisymmetric spin-orbit coupling (ASOC), which may lift the spin degeneracy and give rise to both spin-singlet and spin-triplet components in the order parameter.[1] On the other hand, the strength of ASOC is crucial to generate the mixed singlet-triple pairing. For example, Li_2Pd_3B is well known as a fully gapped s-wave superconductor,[2–4] whereas Li_2Pt_3B with stronger ASOC is a nodal superconductor.[4–7] Accordingly, noncentrosymmetric superconductors often exhibit many unconventional superconducting behaviors, such as multigap superconductivity, nodal superconductivity, and large upper critical field that exceeds the Pauli paramagnetic limit, etc.[8–12]

Notably, some noncentrosymmetric superconductors also display time-reversal symmetry breaking (TRSB) in the superconducting state,[13–17] though time reversal symmetry and spatial inversion symmetry are independent of each other. For instance, various α-Mn-type Re-based noncentrosymmetric superconductors, such as Re_6Zr,[13] Re_6Hf,[15] $Re_{24}Ti_5$,[17] $Re_{0.82}Nb_{0.18}$,[18] exhibit TRSB, even though some studies suggested conventional fully gaped superconducting states.[19,20] Interestingly, it has been recently shown that Re metal also possesses TRSB in its superconducting state, while the crystalline structure of Re metal is centrosymmetric.[18] In contrast, TRSB is absent in the isostructural noncentrosymmetric superconductors $Nb_{0.5}Os_{0.5}$[21] and $Mg_{10}Ir_{19}B_{16}$.[22] Thus, it was suggested that the local electronic structure of Re plays a crucial role in determining the TRSB in the superconducting states of Re metal and Re-based noncentrosymmetric compounds ReM (M refers to transition metals).[18] In other words, the occurrence of TRSB in these Re-based materials was suggested to be independent of M. However, such argument cannot account for the recent findings of an absence of TRSB in isostructural noncentrosymmetric superconductors Re_3Ta[23] and Re_3W.[24] Therefore, it is desirable to systematically vary Re content in Ta_xRe_{1-x} or W_xRe_{1-x} to further examine the role of local electronic structure of both Re and Ta(or W) on TRSB in the superconducting state, compared to compounds with Re alloyed with adjacent Nb, Zr, Ti, Hf. Given that there are two different crystalline structures in Re_3W,[24] i.e., noncentrosymmetric and centrosym-

Supported by the National Key R&D Program of China (Grant No. 2018YFA0704300), the National Natural Science Foundation of China (Grant Nos. U1732162, 11974061, 11704047, U1832147 and 11674054), and the Strategic Priority Research Program (B) of the Chinese Academy of Sciences (Grant No. XDB25000000).
*Corresponding authors. Email: zxshi@seu.edu.cn; kexiangl@msu.edu; pabitra.biswas@stfc.ac.uk
© 2021 Chinese Physical Society and IOP Publishing Ltd

metric, we hence choose Ta_xRe_{1-x} as an object of this study.

In this Letter, we investigate the superconducting properties of a series of Ta_xRe_{1-x} ($0.1 \leq x \leq 0.25$) samples with various Re contents by means of magnetic susceptibility, electrical resistivity, heat capacity, and muon-spin rotation and relaxation measurements. All these samples studied exhibit noncentrosymmetric crystal structure and become superconducting at low temperature with a maximum $T_c \sim 8$ K for $x = 0.15$. Intriguingly, the $Ta_{0.15}Re_{0.85}$ system in our study, which is probably an enhanced ASOC than $Nb_{0.18}Re_{0.82}$ as well as is composed of local electronic structure of Re superconductor, does not show TRSB, which is distinct from many other ReM compounds. It is likely that not only the local electronic structure of Re is crucial, the 5d bands of Ta with enhanced SOC also play a key role in determining the superconducting state of this system, which warrants further investigation.

Polycrystalline Ta_xRe_{1-x} samples were coined by arc melting stoichiometric amounts of tantalum shots and rhenium pieces (all 99.99% pure). To ensure phase homogeneity, we flipped and remelted the materials several times, and then annealed at 1273 K in vacuumed quartz tube no less than 9 days. The powder x-ray diffraction (XRD) data was obtained using a Rigaku diffractometer with Cu $K\alpha$ radiation and a graphite monochromator. The heat capacity was measured using a Quantum Design physical property measurement system (QD-PPMS-9T), and magnetic susceptibility was measured using a Quantum Design magnetic property measurement system (QD-MPMS-7T).

Zero-field (ZF), longitudinal-field (LF), and transverse-field (TF) muon-spin rotation and relaxation (μSR) measurements were performed on the MUSR instrument at the ISIS pulsed muon source. The polycrystalline sample in the form of powder was mounted on a highly pure silver sample holder. The sample was cooled from above T_c to the base temperature at $H = 0$ in ZF-μSR measurements and a field of 300 Oe in TF-μSR measurements. The typical counting statistics were ~30 million muon decays per data point. The ZF- and TF-μSR data were analyzed using the equations described in the text.

All Ta_xRe_{1-x} samples studied in this work crystallize in the α-Mn cubic structure with space group $I\bar{4}3m$ (No. 217). The XRD pattern of polycrystalline Ta_xRe_{1-x} samples is shown in Fig. 1(a). A systematic shift of the diffraction peaks to lower angles with increasing x is observed, indicating that the size of the crystal lattice increases. To extract the lattice parameters, we carry out Rietveld refinement of the powder XRD patterns for each Ta_xRe_{1-x} sample. Figure 1(b) shows a typical example of the Rietveld refinement result of $Ta_{0.15}Re_{0.85}$. The obtained unit cell volume based on the refinements is shown in Fig. 1(d). As is seen, the unit cell volume increases with increasing x, in agreement with the larger atomic radius of Ta compared to Re.

The temperature dependence of magnetic susceptibility measured under a field of 1 mT with different x values is shown in Fig. 1(c). The sharp superconducting transitions suggest excellent homogeneity of samples. The transition temperature T_c as a function of x is shown in Fig. 1(d). One can see that T_c varies non-monotonically with x, with a maximum $T_c \sim 8$ K at the optimal Ta substitution with $x = 0.15$. Note that T_c of Ta_xRe_{1-x} with $x = 0.25$ is in agreement with that of Re_3Ta in a very recent report by Barker *et al.*[23]

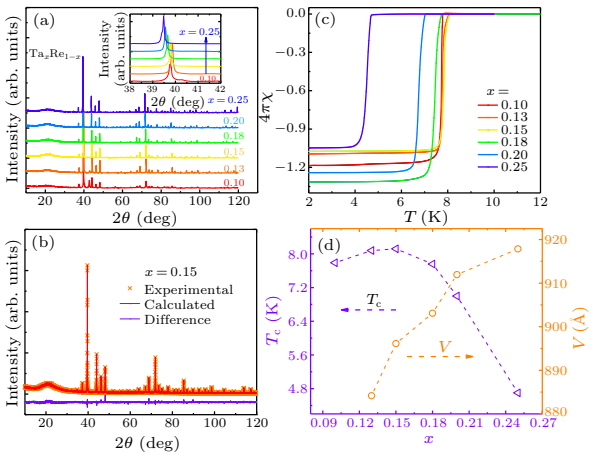

Fig. 1. (a) Powder XRD pattern at room temperature for Ta_xRe_{1-x} (x = 0.13, 0.15, 0.18, 0.20, 0.25). The inset is an enlarged view of the main diffraction peak of these compounds. (b) Rietveld refinement of the powder XRD of $Ta_{0.15}Re_{0.85}$. (c) Temperature dependence of magnetic susceptibility $\chi(T)$ for Ta_xRe_{1-x}(x = 0.1, 0.13, 0.15, 0.18, 0.20, 0.25) with zero-field cooling (ZFC). (d) T_c and the unit cell volume vs Ta content x.

Figure 2(a) presents the temperature dependence of the heat capacity of $Ta_{0.15}Re_{0.85}$. The large specific heat jump at T_c confirms the bulk superconductivity. The normal-state heat capacity can be nicely fitted using the Debye model $C/T = \gamma_n + \beta T^2 + \delta T^4$, as illustrated by the red curve, from which we extract the Sommerfeld constant $\gamma_n = 4.64\,\text{mJ}\cdot\text{mol}^{-1}\cdot\text{K}^{-2}$, $\beta = 0.033\,\text{mJ}\cdot\text{mol}^{-1}\cdot\text{K}^{-4}$, and $\delta = 0.00028\,\text{mJ}\cdot\text{mol}^{-1}\cdot\text{K}^{-6}$. Figure 2(b) shows the temperature dependence of heat capacity measured in the presence of magnetic fields ranging between 0 T and 9 T. As is expected, the superconducting transition temperature is gradually suppressed with increasing magnetic field. By fitting all the specific heat data in the superconducting state measured with different magnetic fields using the Debye model described above, we can extract the electronic term contributing to specific heat, $\gamma(H)$. In Fig. 2(c), we plot the $\Delta\gamma(H)$ [$\Delta\gamma(H) = \gamma(H) - \gamma(0\,\text{T})$] versus magnetic field. One can see that $\Delta\gamma(H)$ exhibits nearly linear field dependence, which has been observed in nodeless superconductors such as $Ca_3Ir_4Sn_{13}$,[25] implying the nodeless gap in $Ta_{0.15}Re_{0.85}$. We further analyze its low-temperature zero-field heat capacity ΔC by subtracting the heat capacity based on the fitting to normal state heat ca-

pacity data from the measured data shown in Fig. 2(a). The temperature dependence of ΔC is presented in Fig. 2(c), which is modeled using different gap functions, and we adopt the α-model for the temperature dependence of the gap functions (see, e.g., Refs. [26,27]). As shown in Fig. 2(c) and 2(d), while both the single-gap s-wave and two-gap s-wave model can fit the data, the two-gap s-wave better compared to the one-gap s-wave model. In Table 1, we list the parameters based on each gap function fitting. The extracted $\Delta C/\gamma_n T_c$ is found to be 1.61, which is larger than the theoretical value (1.43) of the well-known BCS theory. For the two-gap s-wave model, the gap to T_c ratio, $\Delta_1(0)/k_B T_c = 1.2$ and $\Delta_2(0)/k_B T_c = 2.1$, the latter of which is larger than BCS of 1.76. This indicates one superconducting gap is weakly electron-phonon coupled, while the other is in the strong coupling limit.

Table 1. Fit parameters obtained using different models of SC pairing symmetry [see Fig. 4(c)].

Model	α	γ_n (mJ·mol^{-1}·K^{-2})	Gap value [$\Delta(0)$ (meV)]	Gap ratio
One s-wave	1.07	4.7	1.3	1.9
Two s-waves	(0.68, 1.2)	(0.85, 3.5)	(0.81, 1.44)	(1.2, 2.1)

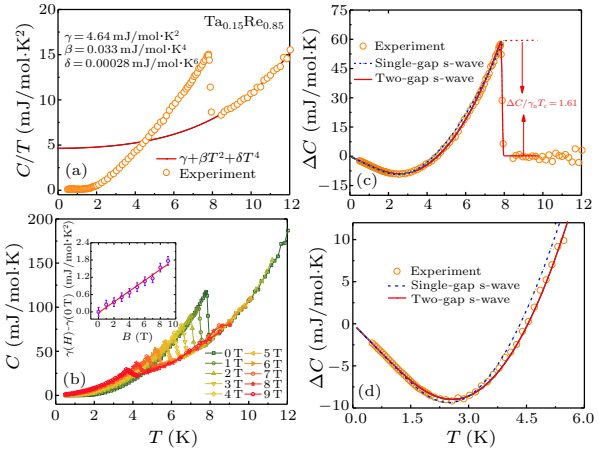

Fig. 2. Specific heat capacity of $Ta_{0.15}Re_{0.85}$. (a) Temperature dependence of heat capacity, plotted as C/T versus T. The red solid line is a fit based on $C/T = \gamma_n + \beta T^2 + \delta T^4$ for $Ta_{0.15}Re_{0.85}$. (b) Low-temperature specific heat C vs T in a set of stable magnetic fields up to 9 T. The inset shows field dependence of Sommerfeld coefficient $\Delta\gamma(H) = \gamma(H) - \gamma(0\,\mathrm{T})$. (c) The fitting of ΔC versus T using different gap-symmetry functions. Here $\Delta C = C - C_n$, with C_n is the heat capacity in the normal state. (d) The enlarged view of lower temperature range of (c).

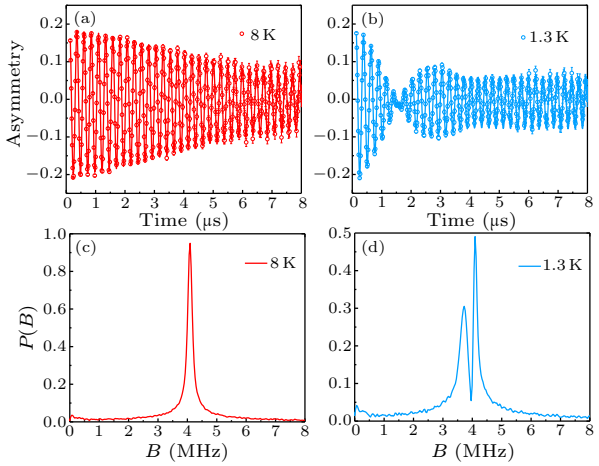

Fig. 3. TF-μSR time spectra of $Ta_{0.15}Re_{0.85}$ collected at (a) 8 and (b) 1.3 K in a transverse field of 30 mT. The solid lines are the fits to the data using Eq. (1), described in the text. [(c), (d)] The fast Fourier transform of the TF-μSR time spectra, collected at 8 and 1.3 K, respectively.

Superconducting properties of $Ta_{0.15}Re_{0.85}$ were further investigated from the TF-μSR measurements. The main aim was to calculate the temperature dependence of the superfluid density and the absolute value of the penetration depth λ. The temperature dependence of the superfluid density can provide crucial information about the superconducting gap values and identify the symmetry of the gap structure. TF measurements were performed in a magnetic field of 30 mT. Note that this measured field is much smaller than the upper critical field obtained via resistivity measurements under a set of field (data not shown). Figure 3 shows the TF-μSR time spectra at (a) 8 and (b) 1.3 K. The 8 K data shows only very weak relaxation rate, contributed by the nuclear moments in the material. By contrast, the 1.3 K data shows much higher relaxation due to the inhomogeneous field distribution dominated by the vortex lattice in the superconducting state. Figures 3(c) and 3(d) show the fast Fourier transform of the TF-μSR time spectra, collected at 8 and 1.3 K, respectively. As is expected, we see a sharp single peak in the probability field distribution $p(B)$ at 8 K, corresponding to the applied field frequency only. However, data collected at 1.3 K show two peaks in $p(B)$. One is at the applied field frequency due to some muons missing the sample and hitting the sample holder. The other peak is at a frequency lower then the applied field frequency, representing the field distribution of the vortex lattice in the superconducting mixed state of $Ta_{0.15}Re_{0.85}$. All the TF-μSR time spectra were analyzed using a spin precession signal with Gaussian type relaxation function along with a non-relaxing background contribution as follows:

$$A^{\mathrm{TF}}(t) = A(0)\exp(-\sigma^2 t^2/2)\cos(\gamma_\mu \langle B\rangle t + \phi) + A_{\mathrm{bg}}\cos(\gamma_\mu B_{\mathrm{bg}} t + \phi), \quad (1)$$

where $A(0)$ and A_{bg} are the initial asymmetry of TF-μSR time spectra of the muons are hitting and missing the sample, respectively; $\gamma_\mu/2\pi = 13.55$ kHz/G is the muon gyromagnetic ratio,[28] $\langle B\rangle$ and B_{bg} are the internal and background magnetic fields, respectively; ϕ is the initial phase of the muon precession signal; and σ is the Gaussian muon spin relaxation rate. The

non-relaxing background signal is mainly due to some muons missing the sample and hitting the silver sample holder which has very low nuclear moments.

Figure 4(a) presents the temperature dependence of σ and internal field of $Ta_{0.15}Re_{0.85}$, extracted from the analysis of the TF-μSR time spectra as discussed above. Here, $\sigma(T)$ shows a sudden change in slope just below T_c. This indicates that the sample is in superconducting mixed state. We also see a strong diamagnetic shift in the temperature dependence of the internal field data, which indicates the bulk nature of superconductivity in $Ta_{0.15}Re_{0.85}$. The Gaussian muon spin relaxation rate σ can be expressed as $\sigma = (\sigma_{sc}^2 + \sigma_{nm}^2)^{\frac{1}{2}}$, where σ_{sc} is due to the inhomogeneous field distribution in the vortex state, and $\sigma_{nm} = 0.296(4)\,\mu s^{-1}$ is the nuclear contribution and is considered to be temperature independent.

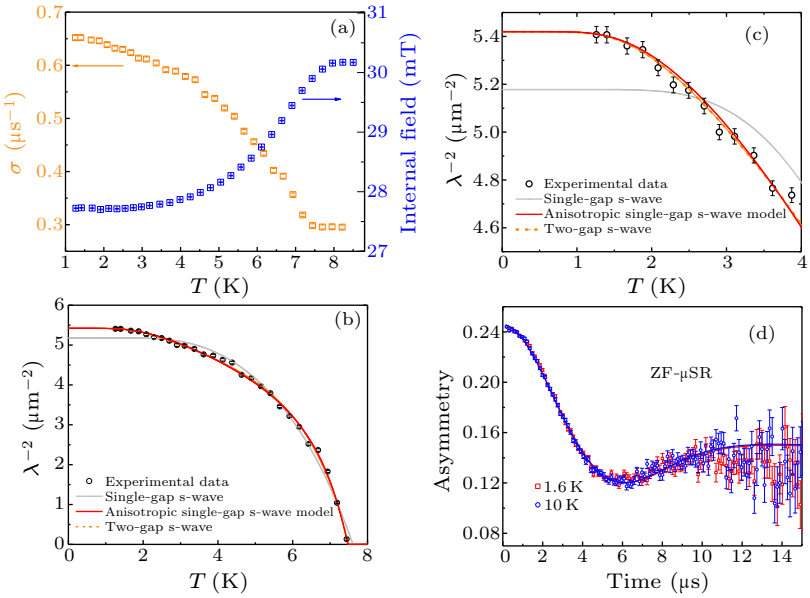

Fig. 4. (a) The temperature dependence of σ and internal field of $Ta_{0.15}Re_{0.85}$ for the data collected in an applied field of 30 mT under field cooled condition. (b) Temperature dependence of λ^{-2} for $Ta_{0.15}Re_{0.85}$. The curves are fits to the data using a single-, an anisotropic single-gap and a two-gap s-wave model. (c) The enlarged view of panel (b). (d) ZF-μSR time spectra collected at 1.6 K and 10 K for $Ta_{0.15}Re_{0.85}$. The solid lines are the fits to the data using Eq. (5), described in the text.

If the applied field much smaller than the upper critical field, i.e., $H \ll H_{c2}$, then σ_{sc} is related to the penetration depth, λ by a simplified Brandt equation,[29] based on the Ginzburg–Landau treatment of the vortex state of a type-II superconductor, as follows:

$$\frac{\sigma_{sc}(T)}{\gamma_\mu} = 0.06091\frac{\Phi_0}{\lambda^2(T)}. \quad (2)$$

Here, $\Phi_0 = 2.068 \times 10^{-15}$ Wb is the flux quantum; $\lambda^{-2}(T)$ is proportional to the effective superfluid density; ρ_s hence can be modeled to identify the symmetry of the superconducting gap.

The temperature dependence of λ^{-2} of $Ta_{0.15}Re_{0.85}$ is shown in Fig. 4(b). Here $\lambda^{-2}(T)$ shows saturation below $T_c/3$, which is strongly suggested for nodeless superconductivity in $Ta_{0.15}Re_{0.85}$; $\lambda^{-2}(T)$ fits a single- and a two-gap s-wave model using the following functional form:[30,31]

$$\frac{\lambda^{-2}(T)}{\lambda^{-2}(0)} = \omega\frac{\lambda^{-2}(T,\Delta_{0,1})}{\lambda^{-2}(0,\Delta_{0,1})} + (1-\omega)\frac{\lambda^{-2}(T,\Delta_{0,2})}{\lambda^{-2}(0,\Delta_{0,2})}, \quad (3)$$

where $\lambda(0)$ is the magnetic penetration depth at $T = 0$ K, $\Delta_{0,i}$ is the value of the ith ($i = 1$ or 2 for two-gap model) superconducting gap at $T = 0$ K, ω and $(1-\omega)$ are the weighting factors of the first and second gaps, respectively. Each term in Eq. (3) can be expressed within the local London approximation ($\lambda \gg \xi$)[32,33] as follows:

$$\frac{\lambda^{-2}(T,\Delta_{0,i})}{\lambda^{-2}(0,\Delta_{0,i})} = 1 + \frac{1}{\pi}\int_0^{2\pi}\int_{\Delta(T,\varphi)}^{\infty}\left(\frac{\partial f}{\partial E}\right)\frac{EdEd\varphi}{\sqrt{E^2-\Delta_i(T,\varphi)^2}}, \quad (4)$$

where $f = [1+\exp(E/k_BT)]^{-1}$ is the Fermi function, φ is the angle along the Fermi surface, and $\Delta_i(T,\varphi) = \Delta_{0,i}\delta(T/T_c)g(\varphi)$, with $g(\varphi)$ representing the angular dependence of the gap. The value of $g(\varphi)$ is 1 for signal-gap s-wave and two-gap s-wave models, and $(s+\cos 4\varphi)$ for anisotropic s-wave gap. $\Delta(T)$ can be approximated to $\delta(T/T_c) = \tanh\{1.82[1.018(T_c/T-1)]^{0.51}\}$.[31]

Figures 4(b) and 4(c) are the fits to the $\lambda^{-2}(T)$ data using the different gap models. Table 2 summarizes all the fitted parameters. In the lower temperature, the single-gap s-wave fitting deviates from the experimental data. To the contrary, the data can be fitted nicely with a two-gap s-wave gap model even with an anisotropic s-wave gap model. This suggests that $Ta_{0.15}Re_{0.85}$ is probably a two-gap or

an anisotropic gap superconductor. For the two-gap scenario, similar multi-gap superconductivity has also been observed in many other materials. A few prominent examples are MgB_2, $NbSe_2$, $Lu_2Fe_3Si_5$ and the layered Fe-based superconductors,[34–41] and the fit yields $\lambda(0) = 430(15)$ nm. The gap to T_c ratio, $\Delta_1(0)/k_BT_c = 1.18(5)$ and $\Delta_2(0)/k_BT_c = 3.22(4)$. The ratio of the BCS value of the gap to T_c is 1.76. Comparing these values we can speculate that the bands opening the larger superconducting gap are in strong-coupling limit, whereas the bands opening the smaller gap is in the weak-coupling limit.

Table 2. Fitted parameters of the fits to the $\lambda^{-2}(T)$ data of $Ta_{0.15}Re_{0.85}$ using different models.

Model	Gap value $\Delta(0)$ (meV)	Gap ratio $\Delta(0)/k_BT_c$	χ^2_{reduced}
Single-gap s-wave	1.58(1)	2.40(1)	4.36
Two-gap s-wave	0.76(03), 2.08(3) with $\omega = 0.94(1)$	1.18(5), 3.22(4)	1.07
Aniso s-wave	1.79(01) with $a = 0.63(1)$	2.78(2)	1.10

ZF-μSR measurements were performed to investigate the magnetic properties of $Ta_{0.15}Re_{0.85}$ at a microscopic level. Special attention was given to search for any spontaneous magnetization arising in the superconducting state of this material which can be associated with time-reversal-symmetry (TRS) breaking superconductivity. Figure 4(d) shows the ZF-μSR time spectra of $Ta_{0.15}Re_{0.85}$, collected above and below T_c. Asymmetry parameters in both data sets show very similar time dependence, which indicates that there is no additional magnetism appearing in the superconducting state of $Ta_{0.15}Re_{0.85}$. This implies that the superconducting state $Ta_{0.15}Re_{0.85}$ is less possible to break TRS. The ZF data can be fitted well using a Kubo–Toyabe relaxation function[42] multiplied by an exponential decay term as follows:

$$A(t) = A(0)\Big\{\frac{1}{3} + \frac{2}{3}(1 - a^2t^2)\exp\Big(-\frac{a^2t^2}{2}\Big)\Big\} \cdot \exp(-\Lambda t) + A_{\text{bg}}, \quad (5)$$

where $A(0)$ and A_{bg} are the initial and background asymmetries of the ZF-μSR time spectra, and a and Λ are muon spin relaxation rates due to nuclear and electronic moments, respectively; a was kept as a common parameter in the data analysis as we could see that the nuclear contribution to the muon spin relaxation was nearly temperature independent. The fits yield $a = 0.282(1)$ μs^{-1}, $\Lambda(2K) = 0.038(2)$ μs^{-1}, and $\Lambda(10K) = 0.036(3)$ μs^{-1}. The value of a extracted from the fits reflects the presence of random local fields arising from the nuclear moments within $Ta_{0.15}Re_{0.85}$. The very similar values of Λ above and below T_c are consistent with the presence of diluted and randomly oriented electronic moments most probably arising from impurities and confirm that $Ta_{0.15}Re_{0.85}$ does not break TRS.

Consistent with the previous μSR investigation on Re_3Ta,[23] our study further makes a strong case for the absence of TRSB in $Ta_{0.15}Re_{0.85}$, the member with maximum T_c in these Ta–Re alloys. This appears to suggest the lack of TRSB in the whole series of this Ta–Re family, in sharp contrast to its homologue $Re_{0.82}Nb_{0.18}$ and the elemental Re superconductors. Importantly, our study suggests that, apart from the *local electronic structure* of Re, the transition metal in ReT (T refers to transition metals) also plays an important role in its ground state. The microscopic origin for the discrepancy between ReTa and ReNb, however, merits further theoretical insights.

In summary, we have synthesized a series of noncentrosymmetric alloys Ta_xRe_{1-x} (x = 0.1, 0.13, 0.15, 0.18, 0.2, 0.25) and constructed the corresponding phase diagram of alloying. The analysis of both heat capacity and μSR data indicates the two-gap order parameter in its superconducting state, one of strong coupling nature and the other weakly coupled. Moreover, muon-spin rotation and relaxation measurements demonstrate the absence of TRSB in the superconducting state of $Ta_{0.15}Re_{0.85}$, in contrast to the TRSB recently observed in Re–Nb alloys.

References

[1] Smidman M, Salamon M B, Yuan H Q and Agterberg D F 2017 *Rep. Prog. Phys.* **80** 036501
[2] Nishiyama M, Inada Y and Zheng G Q 2005 *Phys. Rev. B* **71** 220505(R)
[3] Takeya H, Hirata K, Yamaura K, Togano K, Massalami M E, Rapp R, Chaves F A and Ouladdiaf B 2005 *Phys. Rev. B* **72** 104506
[4] Yuan H Q, Agterberg D F, Hayashi N, Badica P, Vandervelde D, Togano K, Sigrist M and Salamon M B 2006 *Phys. Rev. Lett.* **97** 017006
[5] Nishiyama M, Inada Y and Zheng G Q 2007 *Phys. Rev. Lett.* **98** 047002
[6] Takeya H, Massalami M E, Kasahara S and Hirata K 2007 *Phys. Rev. B* **76** 104506
[7] Harada S, Zhou J J, Yao Y G, Inada Y and Zheng G Q 2012 *Phys. Rev. B* **86** 220502(R)
[8] Bao J K, Liu J Y, Ma C W, Meng Z H, Tang Z T, Sun Y L, Zhai H F, Jiang H, Bai H, Feng C M, Xu Z A and Cao G H 2015 *Phys. Rev. X* **5** 011013
[9] Guan S Y, Chen P J, Chu M W, Sankar R, Chou F C, Jeng H T, Chang C S and Chuang T M 2016 *Sci. Adv.* **2** e1600894
[10] Carnicom E M, Xie W W, Klimczuk T, Lin J J, Górnicka K, Sobczak Z, Ong N P and Cava R J 2018 *Sci. Adv.* **4** eaar7969
[11] Mayoh D A, Hillier A D, Götze K, Paul D M, Balakrishnan G and Lees M R 2018 *Phys. Rev. B* **98** 014502
[12] Górnicka K, Gui X, Wiendlocha B, Nguyen L T, Xie W W, Cava R J and Klimczuk T 2020 *Adv. Funct. Mater.* 2007960
[13] Singh R P, Hillier A D, Mazidian B, Quintanilla J, Annett J F, Paul D M, Balakrishnan G and Lees M R 2014 *Phys. Rev. Lett.* **112** 107002
[14] Bauer E, Sekine C, Sai U, Rogl P, Biswas P K and Amato A 2014 *Phys. Rev. B* **90** 054522
[15] Singh D, Barker J A T, Thamizhavel A, Paul D M, Hillier A D and Singh R P 2017 *Phys. Rev. B* **96** 180501(R)
[16] Singh D, Sajilesh K P, Barker J A T, Paul D M, Hillier A D and Singh R P 2018 *Phys. Rev. B* **97** 100505(R)
[17] Shang T, Pang G M, Baines C, Jiang W B, Xie W, Wang A, Medarde M, Pomjakushina E, Shi M, Mesot J, Yuan H Q and Shiroka T 2018 *Phys. Rev. B* **97** 020502(R)
[18] Shang T, Smidman M, Ghosh S K, Baines C, Chang L J, Gawryluk D J, Barker J A T, Singh R P, Paul D M, Bal-

akrishnan G, Pomjakushina E, Shi M, Medarde M, Hillier A D, Yuan H Q, Quintanilla J, Mesot J and Shiroka T 2018 *Phys. Rev. Lett.* **121** 257002
[19] Matano K, Yatagai R, Maeda S and Zheng G Q 2016 *Phys. Rev. B* **94** 214513
[20] Pang G M, Nie Z Y, Wang A, Singh D, Xie W, Jiang W B, Chen Y, Singh R P, Smidman M and Yuan H Q 2018 *Phys. Rev. B* **97** 224506
[21] Singh D, Barker J A T, Arumugam T, Hillier A D, Paul D M and Singh R P 2018 *J. Phys.: Condens. Matter* **30** 075601
[22] Aczel A A, Williams T J, Goko T, Carlo J P, Yu W, Uemura Y J, Klimczuk T, Thompson J D, Cava R J and Luke G M 2010 *Phys. Rev. B* **82** 024520
[23] Barker J A T, Breen B D, Hanson R, Hillier A D, Lees M R, Balakrishnan G, Paul D M and Singh R P 2018 *Phys. Rev. B* **98** 104506
[24] Biswas P K, Hillier A D, Lees M R and Paul D M 2012 *Phys. Rev. B* **85** 134505
[25] Wang K F and Petrovic C 2012 *Phys. Rev. B* **86** 024522
[26] Xu X, Chen B, Jiao W H, Chen B, Niu C Q, Li Y K, Yang J H, Bangura A F, Ye Q L, Cao C, Dai J H, Cao G and Hussey N E 2013 *Phys. Rev. B* **87** 224507
[27] Xu C Q, Li B, Feng J J, Jiao W H, Li Y K, Liu S W, Zhou Y X, Sankar R, Zhigadlo N D, Wang H B, Han Z D, Qian B, Ye W, Zhou W, Shiroka T, Biswas P K, Xu X F and Shi Z X 2019 *Phys. Rev. B* **100** 134503
[28] Sonier J E, Brewer J H and Kiefl R F 2000 *Rev. Mod. Phys.* **72** 769
[29] Brandt E H 2003 *Phys. Rev. B* **68** 054506
[30] Padamsee H, Neighbor J E and Shiffman C A 1973 *J. Low Temp. Phys.* **12** 387
[31] Carrington A and Manzano F 2003 *Physica C* **385** 205
[32] Tinkham M 1975 *Introduction to Superconductivity* (New York: McGraw-Hill)
[33] Prozorov R and Giannetta R W 2006 *Supercond. Sci. Technol.* **19** R41
[34] Khasanov R, Conder K, Pomjakushina E, Amato A, Baines C, Bukowski Z, Karpinski J, Katrych S, Klauss H H, Luetkens H, Shengelaya A and Zhigadlo N D 2008 *Phys. Rev. B* **78** 220510(R)
[35] Biswas P K, Balakrishnan G, Paul D M, Tomy C V, Lees M R and Hillier A D 2010 *Phys. Rev. B* **81** 092510
[36] Biswas P K, Krzton-Maziopa A, Khasanov R, Luetkens H, Pomjakushina E, Conder K and Amato A 2013 *Phys. Rev. Lett.* **110** 137003
[37] Paglione J and Greene R L 2010 *Nat. Phys.* **6** 645
[38] Choi H J, Roundy D, Sun H, Cohen M L and Louie S G 2002 *Nature* **418** 758
[39] Yokoya T, Kiss T, Chainani A, Shin S, Nohara M and Takagi H 2001 *Science* **294** 2518
[40] Nakajima Y, Nakagawa T, Tamegai T and Harima H 2008 *Phys. Rev. Lett.* **100** 157001
[41] Biswas P K, Balakrishnan G, Paul D M, Lees M R and Hillier A D 2011 *Phys. Rev. B* **83** 054517
[42] Kubo R 1981 *Hyperfine Interact.* **8** 731